ACS Partner Journal

Journal of the American Society for Mass Spectrometry

pubs.acs.org/jasms

Research Article

Photoelectron Spectroscopic and Computational Study of the Deprotonated Gallic Acid and Propyl Gallate Anions

Zhaoguo Zhu, Mary Marshall, Rachel Harris, Evan Collins, and Kit H. Bowen*

Cite This: https://doi.org/10.1021/jasms.2c00017

Read Online

ACCESS | Metrics & More | Article Recommendations | Supporting Information

ABSTRACT: Antioxidants play important roles in eliminating reactive oxygen species (ROS), which have been associated with various degenerative diseases, such as cancer, aging, and inflammatory diseases. Gallic acid (GA) and propyl gallate (PG) are well-known antioxidants and have been widely studied in vitro and in vivo. The biological antioxidant abilities of GA and PG are related to the electronic structure of their dehydro-radicals. In this work, we report a combined photoelectron spectroscopic and computational study of the deprotonated gallic acid anion, $[GA - H]^-$, and deprotonated propyl gallate anion, $[PG - H]^-$. Adiabatic electron affinities of the dehydro-gallic acid radical, $[GA - H]\cdot$ and of the dehydro-propyl gallate radical, $[PG - H]\cdot$, are measured to be 2.90 ± 0.05 eV and 2.85 ± 0.05 eV, respectively, and compared to computational results.

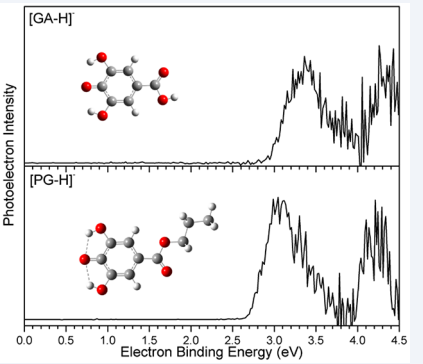

INTRODUCTION

Reactive oxygen species (ROS), primarily generated in the mitochondria of cells, have been regarded as toxic byproducts resulting from metabolism processes involved in cancer and other diseases.[1−4] Common ROS exist in the form of hydroxyl radicals (OH·), alkoxyl radicals (RO·), peroxyl radicals (ROO·), and hydrogen peroxide (H_2O_2).[5] Excessive levels of these species are thought to have destructive consequences on cellular macromolecules, e.g., lipids, proteins, and DNA, resulting in cell and tissue injury that is often associated with degenerative diseases.[6−12] Nutritional and medical studies have identified several antioxidants that prevent the oxidative stress caused by ROS.[13,14] The antioxidants react with ROS faster than relevant biological targets react with ROS, thus protecting lipids, fats, and proteins from the attack of free radicals.

Among the various antioxidants, gallic acid (GA) and its derivative propyl gallate (PG) are thought to possess strong abilities to scavenge ROS.[15,16] Gallic acid, also known as 3,4,5-trihydroxybenzoic acid, is widely present in the plant kingdom and found in various food sources, such as tea, grapes, and red wine.[17−21] Propyl gallate, commonly used as an antioxidant in food, is a synthetic derivative of GA.[22,23] Both of them act as antioxidants, antibacterial agents, antitumor agents, and anti-inflammatory agents in the body.[24−27] The mechanism of action among phenolic antioxidants has been extensively investigated.[28−31] For polyphenols, hydrogen atom transfer (HAT) and single electron transfer (SET) are the two dominant mechanistic pathways.[32,33] They are represented in Figure 1. Via HAT, GA and PG react with free radicals as hydrogen donors and form the relatively stable dehydro-gallate, $[GA - H]\cdot$, and dehydro-propyl gallate, $[PG - H]\cdot$, radicals. In the case of SET, antioxidants lose an electron to the radical first and then undergo the proton transfer process. Previous DFT computational analysis suggested that GA in the gas phase reacts by HAT.[29] In aqueous and lipid media at physiological pH, PG reacts with $^{\cdot}OOH$, $\cdot OOCH_3$, and $^{\cdot}OOCHCH_2$ radicals by transferring the hydrogen from the phenolic hydroxyl(s) group.[34] In particular, the bond dissociation enthalpy (BDE) of O−H bonds has been shown to be a good indicator of antioxidant activity due to the HAT mechanism.[35] The BDE values of O−H bonds for GA and PG are estimated to be 347.4 and 334.6 kJ/mol, respectively, based on the experimentally measured rate constants of reactions of the antioxidants with the lipid peroxy radicals.[36,37] Also, computational investigations of BDE values for GA and PG in different environments have been carried out. The computed BDE values range from 318 to 385 kJ/mol for GA and from 297 to 371 kJ/mol for PG.[28,37−43]

However, despite results from decades of spectroscopic and theoretical studies on the antioxidant capabilities and stabilities of GA and PG, the electron affinity (EA) values of the $[GA - H]\cdot$ and the $[PG - H]\cdot$ radicals had not been measured.[44−48] These EA values would be particularly useful, however, because they could be used to determine O−H BDE values in the acidity/electron affinity thermochemical cycle proposed

Special Issue: Focus: Gas-Phase Ion Chemistry

Received: January 18, 2022
Revised: February 16, 2022
Accepted: February 23, 2022

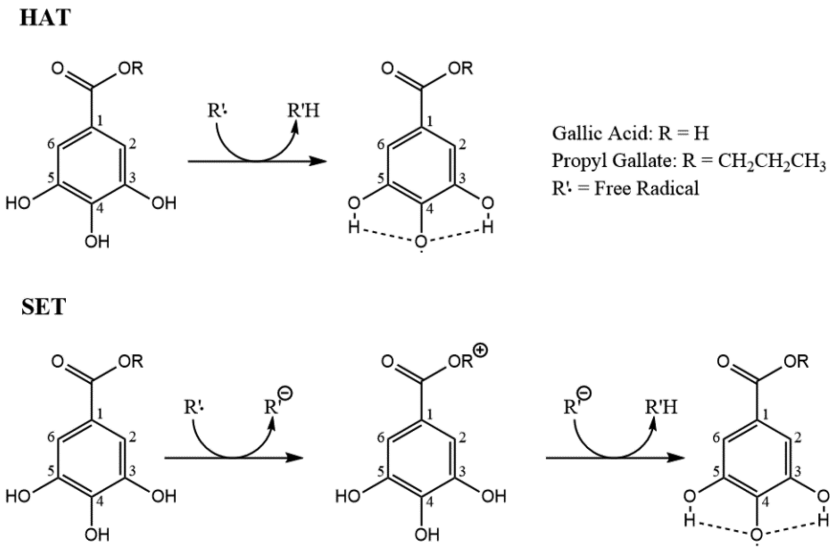

Figure 1. HAT and SET mechanisms of the radical scavenging process.

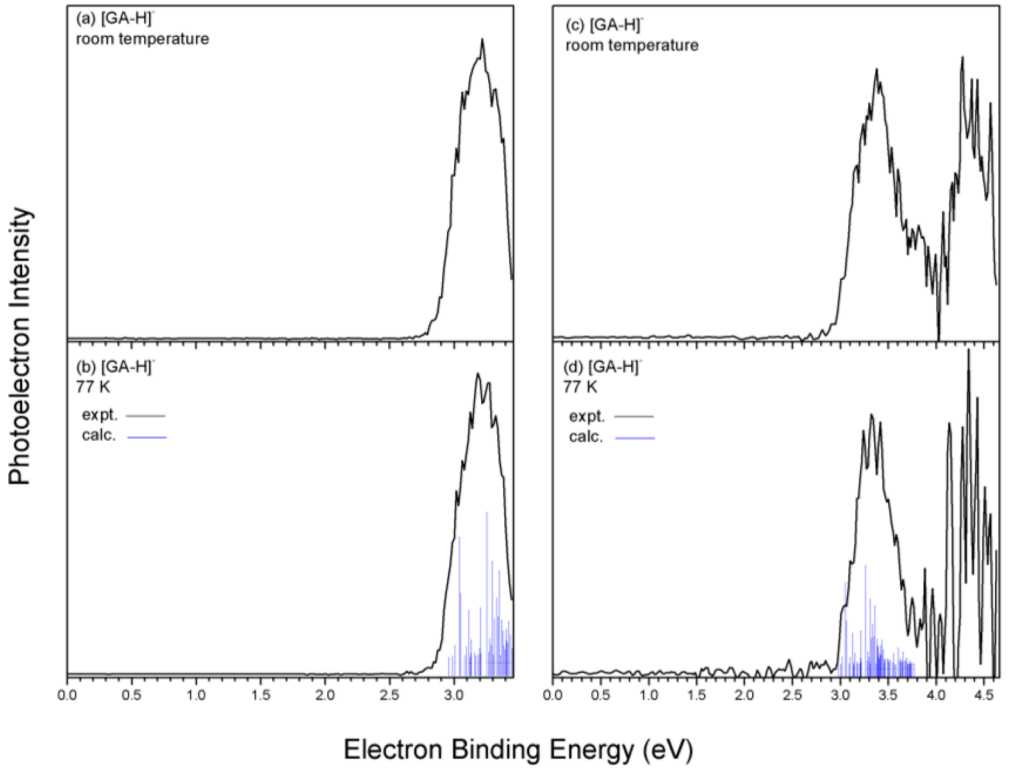

Figure 2. Photoelectron spectra of $[GA - H]^-$ recorded with (a) 3.49 eV photons at room temperature, (b) 3.49 eV photons at 77 K, (c) 4.66 eV photons at room temperature, and (d) 4.66 eV photons at 77 K.

by Blanksby and Ellison.[49] Knowledge of O−H BDE values can provide insight into the antioxidant nature of GA and PG, as they have for other radical scavengers, such as vitamin E and vitamin C. Here we present our experimental and computational studies of the electronic structure of $[GA - H]\cdot$ and $[PG - H]\cdot$. The experimental part of this work involved forming their anions through electrospray ionization and measuring their anion photoelectron spectra. This led to the determination of the electron affinities and excitation energies of the $[GA - H]\cdot$ and $[PG - H]\cdot$ radicals, which were then compared to results from our computations. This work takes its place alongside previous anion photoelectron spectroscopic studies of vitamin E and vitamin C.[50,51]

METHODS

Experimental Section. Deprotonated gallate anions, $[GA - H]^-$, and deprotonated propyl gallate anions, $[PG - H]^-$, were generated via electrospray ionization, one of the anion sources on our existing pulsed anion photoelectron spectrometer. Details of the electrospray ionization source have been described elsewhere previously.[51] Millimolar solutions of propyl gallate (Sigma-Aldrich, ≥98.0%) in 3:1 MeOH:H_2O were prepared over a range of pH values (9 < pH < 11). These

https://doi.org/10.1021/jasms.2c00017
J. Am. Soc. Mass Spectrom. XXXX, XXX, XXX−XXX

Table 1. Experimentally and Computationally Determined Values for Deprotonated Propyl Gallate and Gallic Acid Anions and Their Corresponding Neutral Radicals (eV)

	expt EA	calcd EA	expt VDE	calcd VDE	expt. first excitation energy[a]	calcd first excitation energy
[GA − H]·/ [GA − H]$^-$	2.90 ± 0.05	2.96	3.32 ± 0.05	3.20	~1.25	1.40
[PG − H]·/ [PG − H]$^-$	2.85 ± 0.05	2.87	3.06 ± 0.05	3.08	~1.30	1.39

[a]This value was obtained by subtracting the VDE from the EBE value of the second peak in the spectrum.

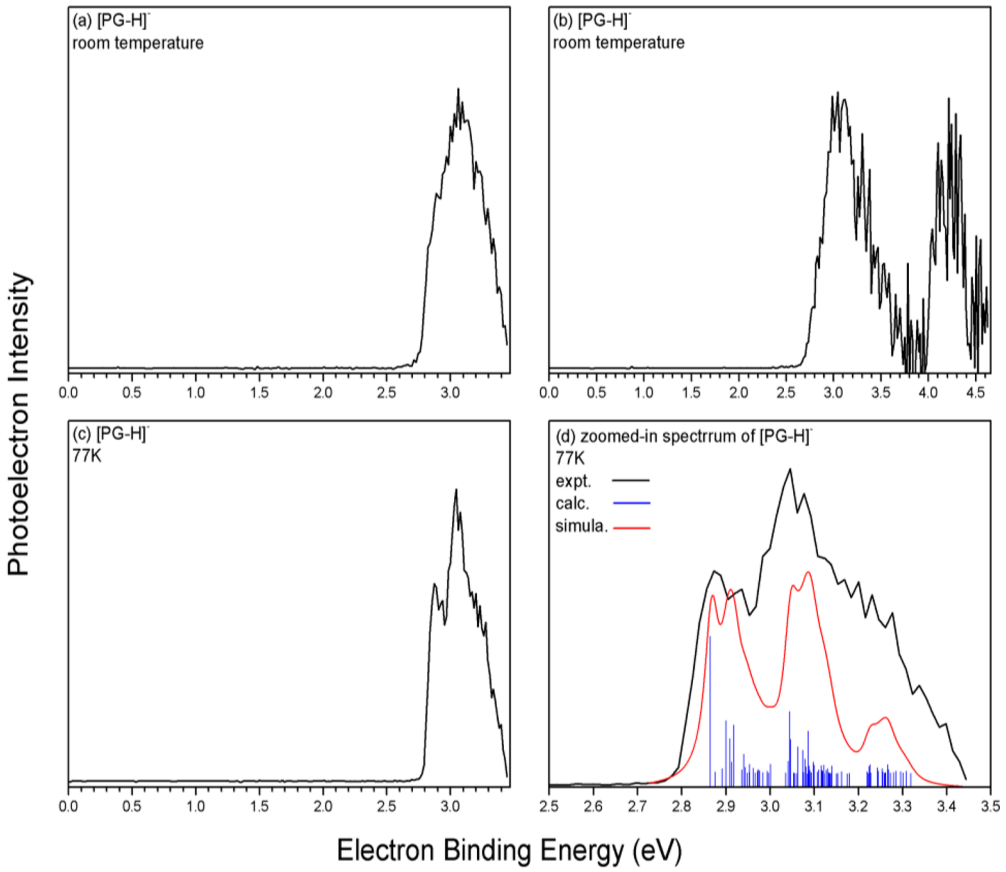

Figure 3. Photoelectron spectra of [PG − H]$^-$ recorded with (a) 3.49 eV photons at room temperature, (b) 4.66 eV photons at room temperature, (c) 3.49 eV photons at 77 K, and (d) an expanded view of (c), beginning at EBE = 2.5 eV.

solutions were injected through a ~10 μm pulled silica capillary, floated at negative 3−5 kV, into a humidity controlled, ambient atmosphere chamber. A buffer gas composed of 20% H_2 with a balance of He was employed in the ion trap to facilitate cooling of the ions, as well as promoting collision focusing. The ions were accumulated and cooled in the trap for 100 ms before being pulsed into a time-of-flight mass spectrometer to be mass-analyzed. The mass spectrum is displayed in Figure S1 of the Supporting Information. The time-of-flight mass spectrometer portion of our apparatus has also been previously described elsewhere.[52]

The anions of interest were then mass-selected and decelerated before entering a magnetic bottle region of our anion photoelectron spectrometer. Anion photoelectron spectroscopy is conducted by crossing the mass-selected beam of negative ions with a fixed frequency photon beam and energy-analyzing the resultant photodetached electrons. These photoelectrons are governed by the energy-conserving relationship: $h\nu$ = EBE + EKE, where $h\nu$ is the photon energy, EBE is the electron binding (photodetachment transition) energy, and EKE is the measured electron kinetic energy. Our magnetic bottle, electron energy analyzer has a resolution of ~50 meV at an EKE of 1 eV. The photoelectron spectra were collected with both the third and fourth harmonic light from a Nd:YAG laser (355, 3.49, and 266 nm, 4.66 eV photons, respectively) and with the ion trap at both ambient (~300 K) temperature and 77 K. The photoelectron spectra were calibrated against the well-known transitions of I^-.[53,54]

Computational. All calculations were performed using the Gaussian 09 program package.[55] DFT calculations were conducted by applying the M06-2X functional with the D3 dispersion correction.[56,57] All geometries, including that of the anions and their corresponding neutral molecules, were fully optimized without any geometrical constraints while using the aug-cc-pVDZ basis set.[58,59] Frequency analyses were carried out for all optimized structures to ensure the absence of imaginary frequencies. The electronic energies were improved by single-point calculations with a larger basis set, i.e., aug-cc-pVTZ, at the optimized geometries. The excitation energies of the neural radicals were obtained by TD-DFT method. Franck−Condon simulations were carried out using the tools available in the PESCAL2016 package.[60,61] The temperature (~77 K) was adjusted to obtain the best match to the experimental spectra.

https://doi.org/10.1021/jasms.2c00017
J. Am. Soc. Mass Spectrom. XXXX, XXX, XXX−XXX

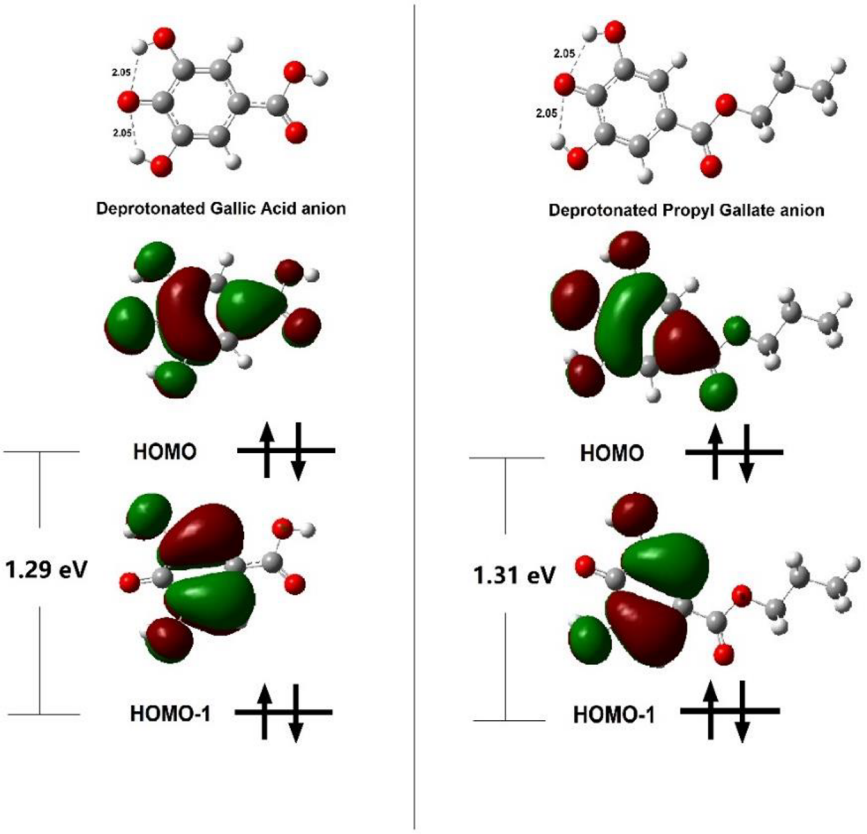

Figure 4. Optimized geometries of $[GA - H]^-$ and $[PG - H]^-$ with their respective HOMO and HOMO−1 molecular orbitals.

RESULTS

Gallic Acid. The photoelectron spectra of the deprotonated gallic acid anion, $[GA - H]^-$, are shown in Figure 2. These spectra were measured at 77 K to reduce the presence vibrational hot bands, i.e., photoelectrons from vibrationally excited anions. A broad EBE band, beginning at EBE = 2.90 eV and reaching its maximum at EBE = 3.32 eV, was observed in all of the spectra. The vertical detachment energy (VDE) is the transition energy, i.e., EBE, at which the Franck−Condon overlap between the wave functions of the anion and its neutral counterpart is greatest. The EBE value corresponding to this maximum intensity in the observed band, i.e., 3.32 eV for the $[GA - H]^-$ anion, is its vertical detachment energy. When significant Franck−Condon overlap exists between $v = 0$ of the anion and $v' = 0$ of its corresponding neutral (the origin transition) and no vibrational hot bands are present, the EBE of the spectrum's threshold value corresponds to the adiabatic electron affinity (EA). The EA is the energy difference between the lowest energy, relaxed geometry of the anion and the lowest energy isomer (global minimum) of its neutral counterpart. By extrapolating the lowest EBE edge, we determine the EA value to be 2.90 ± 0.05 eV. As illustrated in Table 1, our calculated EA = 2.96 eV and VDE = 3.20 eV agree well with the experimental values. In the 266 nm (4.66 eV) spectrum, a second band appears approximately 1.2 eV above the first one. This transition represents photoelectron detachment from an inner molecular orbital. In other words, the second EBE band is also the transition from the ground state of the anion to the first excited state of the neutral radical. After cooling to 77 K, vibrational features spaced by 0.1 eV were also observed at both photon energies. In Figure 2(b) and 2(d), blue stick spectra represent transitions from $v = 0$ of the anion to all of the vibrationally excited states of its corresponding neutral, these being the result of a Franck−Condon analysis.

Propyl Gallate. The photoelectron spectra of the deprotonated propyl gallate anion, $[PG - H]^-$, are presented in Figure 3. These spectra were obtained at the ambient temperature of the ion trap using both 355 nm (3.49 eV) and 266 nm (4.66 eV) photons and at an ion trap temperature of 77 K (to eliminate vibrational hot bands) using 355 nm photons. The ambient temperature 355 nm spectrum consists of a single broad band with a maximum at EBE = 3.06 eV. The ambient temperature 266 nm spectrum reveals a second band, representative of electron detachment from an inner molecular orbital. Upon cooling the ion trap to 77 K, as shown in Figure 3(c), a strong EBE peak at 2.85 eV and its vibrational features are revealed. Figure 3(d) presents an expanded view of Figure 3(c). Displayed in Figure 3(d) is a Franck−Condon simulation-based stick spectrum (in blue) which depicts transitions from $v = 0$ of the anion to all vibrational ground and excited states of its corresponding neutral. The red curve is the simulated spectrum with its features having been subjected to Gaussian broadening of 400 cm^{-1} fwhm. The overall profiles of the experimental and simulated spectra are in good agreement. Additionally, due to the negligible geometrical structure difference between the $[PG - H]^-$ anion and its corresponding neutral radical, $[PG - H]\cdot$, the Franck−Condon overlap between their ground vibrational wave functions is significant, resulting in a strong EA-determining (origin) peak in the spectrum at EBE = 2.85 eV. Our calculated EA = 2.87 and VDE = 3.08 eV values are in excellent

https://doi.org/10.1021/jasms.2c00017
J. Am. Soc. Mass Spectrom. XXXX, XXX, XXX−XXX

agreement with the experimental values, i.e., 2.85 ± 0.05 eV and 3.06 ± 0.05 eV, respectively.

DISCUSSION

Deprotonation of gallic acid can yield three kinds of deprotomers which are carboxylate ion, *p*-phenoxide ion, and *o*-phenoxide ion. Even if the carboxylate isomer had been present, it would not have been observed in the photodetachment spectrum, because its calculated VDE is 4.87 eV and photon energy is 4.66 eV. While it is conceivable that both *o*- and *p*-phenoxide ions can be made by ESI, Boltzmann distribution favors the population of *p*-phenoxide ion of deprotonated gallic acid because *p*-phenoxide ion lies 0.39 eV lower than the ortho one in energy. Additionally, the measured and calculated VDE favors the *p*-phenoxide of gallic acid deprotomer, too. *p*-Phenoxide ion of deprotonated propyl gallate is also thermodynamically preferred due to the large energy gap (0.37 eV) between para and ortho isomers. The geometry and energetics of the isomers are provided in the Figure S2. Figure 4 presents the calculated structures of the most stable conformers of the $[GA - H]^-$ and $[PG - H]^-$ anions, i.e., *p*-phenoxide ions of deprotonated gallic acid and propyl gallate, along with their highest occupied molecular orbitals (HOMO) and their second highest occupied molecular orbitals (HOMO−1). In the left panel of Figure 4, the optimized $[GA - H]^-$ anion structure reveals a singlet ground state and a planar geometry due to conjugation effects. Additionally, two intramolecular hydrogen bonds, each 2.05 Å in length, are formed between two ortho hydroxyl groups and the central oxygen atom on the benzene ring. The neutral $[GA - H]\cdot$ radical also shares a similar geometry with two 2.16 Å intramolecular hydrogen bonds. Intramolecular hydrogen bonds have an enhancing effect on the antioxidant ability, because they stabilize the structure of the $[GA - H]\cdot$ radical and lower the bond dissociation enthalpy of the center O−H bond.[29,49]

The $[PG - H]^-$ anion also forms two intramolecular hydrogen bonds between hydroxyl groups and an oxygen atom of the same length as in the $[GA - H]^-$ anion, i.e., 2.05 Å. However, the neutral $[PG - H]\cdot$ radical has two hydrogen bonds with lengths of 2.16 Å each, which are longer and weaker than its anionic counterpart. We assigned the EBE = 2.85 eV peak to the 0−0 transition, and the VDE = 3.06 eV peak to the transition from the ground state of the anion to a vibrationally excited state in its neutral counterpart, 1262 cm^{-1} above its vibrational ground state. In the 1262 cm^{-1} vibrational mode, two intramolecular hydrogen bonds are stretched, leading to a smaller geometric difference between the anion and neutral, and a larger Franck−Condon overlap.

The HOMO and HOMO−1 molecular orbital structures of $[GA - H]^-$ are both delocalized over the benzene ring and show strong π-like orbital features (Figure 4). The calculated energy difference between these molecular orbitals is 1.29 eV, closely matching the observed interval in the experimental spectrum. The direct detachment feature at EBE values ranging from 2.9 to 3.6 eV corresponds to the loss of an electron from the doubly occupied HOMO in the anion, while the second band, i.e., from 4.0 to 4.5 eV, corresponds to that from HOMO−1. For the $[PG - H]^-$, the energy difference between the HOMO and HOMO−1 is 1.31 eV, which is in accordance with the spacing observed between the two bands in the spectrum taken at 266 nm (Figure 3b). Our TD-DFT calculations also show that the first excited state for both $[GA - H]\cdot$ and $[PG - H]\cdot$ radicals corresponds to the promotion of an electron from HOMO−1 to singly occupied HOMO. The calculated excitation energies of the first excited state are 1.40 and 1.39 eV for $[GA - H]\cdot$ and $[PG - H]\cdot$ radicals, respectively. Additionally, the modest difference in EA values between the $[GA - H]\cdot$ radical (2.90 eV) and the $[PG - H]\cdot$ radical (2.85 eV) is attributed to the small electron density of the HOMO on the propyl group.

CONCLUSION

In this work, the photoelectron spectra of the deprotonated gallic acid anion, $[GA - H]^-$, and the deprotonated propyl gallate anion, $[PG - H]^-$, were measured at both ambient temperature and at 77 K. Electron affinities of the dehydro-gallic acid radical, $[GA - H]\cdot$, as well as of the dehydro-propyl gallate radical, $[PG - H]\cdot$, were determined to be 2.90 ± 0.05 eV and 2.85 ± 0.05 eV, respectively. Our DFT calculations and Franck−Condon analyses confirm the electron affinities and the excitation energies of these two radicals. The measured electron affinity values of these two important antioxidant radicals together with properties, such as acidity and BDE, can provide further insight into their antioxidant natures.

ASSOCIATED CONTENT

Supporting Information

The Supporting Information is available free of charge at https://pubs.acs.org/doi/10.1021/jasms.2c00017.

Details of additional experimental and theoretical results, including the mass spectrum of the propyl gallate solution generated by ESI, optimized conformers of deprotonated gallic acid and propyl gallate, and Cartesian coordinates of selected optimized structures (PDF)

AUTHOR INFORMATION

Corresponding Author

Kit H. Bowen − *Department of Chemistry, Johns Hopkins University, Baltimore, Maryland 21218, United States;* orcid.org/0000-0002-2858-6352; Email: kbowen@jhu.edu

Authors

Zhaoguo Zhu − *Department of Chemistry, Johns Hopkins University, Baltimore, Maryland 21218, United States;* orcid.org/0000-0002-4395-9102

Mary Marshall − *Department of Chemistry, Johns Hopkins University, Baltimore, Maryland 21218, United States;* orcid.org/0000-0001-6614-1963

Rachel Harris − *Department of Chemistry, Johns Hopkins University, Baltimore, Maryland 21218, United States*

Evan Collins − *Department of Chemistry, Johns Hopkins University, Baltimore, Maryland 21218, United States;* Present Address: Intel Corporation, Hillsboro, OR 97124

Complete contact information is available at: https://pubs.acs.org/10.1021/jasms.2c00017

Notes

The authors declare no competing financial interest.

https://doi.org/10.1021/jasms.2c00017
J. Am. Soc. Mass Spectrom. XXXX, XXX, XXX−XXX

■ ACKNOWLEDGMENTS

This material is based upon work supported by the National Science Foundation (NSF) under grant number CHE-2054308 (KHB).

■ ABBREVIATIONS

GA, gallic acid
PG, propyl gallate
[GA − H], dehydro-gallic acid radical
[PG − H], dehydro-propyl gallate radical
$[GA - H]^-$, deprotonated gallic acid anion
$[PG - H]^-$, deprotonated propyl gallate anion

■ REFERENCES

(1) Apel, K.; Hirt, H. Reactive oxygen species: metabolism, oxidative stress, and signal transduction. *Annu. Rev. Plant Biol.* **2004**, *55*, 373−399.
(2) Murphy, M. P. How mitochondria produce reactive oxygen species. *Biochem. J.* **2009**, *417* (1), 1−13.
(3) Turrens, J. F. Mitochondrial formation of reactive oxygen species. *J. Physiol.* **2003**, *552* (2), 335−344.
(4) Yu, B. P. Cellular defenses against damage from reactive oxygen species. *Physiol. Rev.* **1994**, *74* (1), 139−162.
(5) Simon, H. U.; Haj-Yehia, A.; Levi-Schaffer, F. Role of reactive oxygen species (ROS) in apoptosis induction. *Apoptosis.* **2000**, *5* (5), 415−418.
(6) Braekke, K.; Harsem, N. K.; Staff, A. C. Oxidative stress and antioxidant status in fetal circulation in preeclampsia. *Pediatr. Res.* **2006**, *60* (5), 560.
(7) Valko, M.; Rhodes, C.; Moncol, J.; Izakovic, M. M.; Mazur, M. Free radicals, metals and antioxidants in oxidative stress-induced cancer. *Chem.-biol. Interact.* **2006**, *160* (1), 1−40.
(8) Hracsko, Z.; Orvos, H.; Novak, Z.; Pal, A.; Varga, I. S. Evaluation of oxidative stress markers in neonates with intra-uterine growth retardation. *Redox Rep.* **2008**, *13* (1), 11−16.
(9) Harman, E. Protein oxidation in aging and age-related diseases. *J. Gerontology.* **1956**, *11*, 298−300.
(10) Harman, D. The aging process. *Proc. Natl. Acad. Sci. U. S. A.* **1981**, *78* (11), 7124−7128.
(11) Ozawa, T. Genetic and functional changes in mitochondria associated with aging. *Physiol. Rev.* **1997**, *77* (2), 425−464.
(12) Beckman, K. B.; Ames, B. N. The free radical theory of aging matures. *Physiol. Rev.* **1998**, *78* (2), 547−581.
(13) Amarowicz, R.; Pegg, R. B.; Rahimi-Moghaddam, P.; Barl, B.; Weil, J. A. Free-radical scavenging capacity and antioxidant activity of selected plant species from the Canadian prairies. *Food Chem.* **2004**, *84* (4), 551−562.
(14) Halliwell, B.; Aeschbach, R.; Löliger, J.; Aruoma, O. I. The characterization of antioxidants. *Food Chem. Toxicol.* **1995**, *33* (7), 601−617.
(15) Aruoma, O. I.; Murcia, A.; Butler, J.; Halliwell, B. Evaluation of the antioxidant and prooxidant actions of gallic acid and its derivatives. *J. Agric. Food Chem.* **1993**, *41* (11), 1880−1885.
(16) Badhani, B.; Sharma, N.; Kakkar, R. Gallic acid: a versatile antioxidant with promising therapeutic and industrial applications. *RSC Adv.* **2015**, *5* (35), 27540−27557.
(17) Damiani, E.; Bacchetti, T.; Padella, L.; Tiano, L.; Carloni, P. Antioxidant activity of different white teas: comparison of hot and cold tea infusions. *J. Food Compost. Anal.* **2014**, *33* (1), 59−66.
(18) Samanidou, V.; Tsagiannidis, A.; Sarakatsianos, I. Simultaneous determination of polyphenols and major purine alkaloids in Greek Sideritis species, herbal extracts, green tea, black tea, and coffee by high-performance liquid chromatography-diode array detection. *J. Sep. Sci.* **2012**, *35* (4), 608−615.
(19) Schmitzer, V.; Slatnar, A.; Veberic, R.; Stampar, F.; Solar, A. Roasting affects phenolic composition and antioxidative activity of hazelnuts (Corylus avellana L.). *J. Food Sci.* **2011**, *76* (1), S14−S19.
(20) Shahrzad, S.; Aoyagi, K.; Winter, A.; Koyama, A.; Bitsch, I. Pharmacokinetics of gallic acid and its relative bioavailability from tea in healthy humans. *J. Nutr.* **2001**, *131* (4), 1207−1210.
(21) Burns, J.; Gardner, P. T.; O'Neil, J.; Crawford, S.; Morecroft, I.; McPhail, D. B.; Lister, C.; Matthews, D.; MacLean, M. R.; Lean, M. E.; Duthie, G. G.; Crozier, A. Relationship among antioxidant activity, vasodilation capacity, and phenolic content of red wines. *J. Agric. Food Chem.* **2000**, *48* (2), 220−230.
(22) Garrido, J.; Garrido, E. M.; Borges, F. Studies on the food additive propyl gallate: synthesis, structural characterization, and evaluation of the antioxidant activity. *J. Chem. Educ.* **2012**, *89* (1), 130−133.
(23) Becker, L. Final report on the amended safety assessment of propyl gallate. *Int. J. Toxicol.* **2007**, *26*, 89−118.
(24) Ji, B. C.; Hsu, W. H.; Yang, J. S.; Hsia, T. C.; Lu, C. C.; Chiang, J. H.; Yang, J. L.; Lin, C. H.; Lin, J. J.; Suen, L. J. W.; Gibson Wood, W.; Chung, J.-G. Gallic acid induces apoptosis via caspase-3 and mitochondrion-dependent pathways in vitro and suppresses lung xenograft tumor growth in vivo. *J. Agric. Food Chem.* **2009**, *57* (16), 7596−7604.
(25) Kroes, B. V.; van den Berg, A. J. J.; van Ufford, H. C. Q.; van Dijk, H.; Labadie, R. P. Anti-inflammatory activity of gallic acid. *Planta medica.* **1992**, *58* (06), 499−504.
(26) Lee, D. S.; Je, J. Y. Gallic acid-grafted-chitosan inhibits foodborne pathogens by a membrane damage mechanism. *J. Agric. Food Chem.* **2013**, *61* (26), 6574−6579.
(27) Pandurangan, A. K.; Mohebali, N.; Norhaizan, M. E.; Yeng, L. C. Gallic acid attenuates dextran sulfate sodium-induced experimental colitis in BALB/c mice. *Drug Des. Devel. Ther.* **2015**, *9*, 3923.
(28) Lu, Z.; Nie, G.; Belton, P. S.; Tang, H.; Zhao, B. Structure−activity relationship analysis of antioxidant ability and neuroprotective effect of gallic acid derivatives. *Neurochem. Int.* **2006**, *48* (4), 263−274.
(29) Wright, J. S.; Johnson, E. R.; DiLabio, G. A. Predicting the activity of phenolic antioxidants: theoretical method, analysis of substituent effects, and application to major families of antioxidants. *J. Am. Chem. Soc.* **2001**, *123* (6), 1173−1183.
(30) Leopoldini, M.; Pitarch, I. P.; Russo, N.; Toscano, M. Structure, conformation, and electronic properties of apigenin, luteolin, and taxifolin antioxidants. A first principle theoretical study. *J. Phys. Chem. A* **2004**, *108* (1), 92−96.
(31) Marino, T.; Galano, A.; Russo, N. Radical scavenging ability of gallic acid toward OH and OOH radicals. Reaction mechanism and rate constants from the density functional theory. *J. Phys. Chem. B* **2014**, *118* (35), 10380−10389.
(32) Mendes, R. A.; Almeida, S. K.; Soares, I. N.; Barboza, C. A.; Freitas, R. G.; Brown, A.; de Souza, G. L. A computational investigation on the antioxidant potential of myricetin 3, 4′-di-O-α-L-rhamnopyranoside. *J. Mol. Model.* **2018**, *24* (6), 1−8.
(33) Santos, J. L.; Kauffmann, A. C.; da Silva, S. C.; Silva, V. C.; de Souza, G. L. Probing structural properties and antioxidant activity mechanisms for eleocarpanthraquinone. *J. Mol. Model.* **2020**, *26* (9), 1−8.
(34) Medina, M. E.; Iuga, C.; Alvarez-Idaboy, J. R. Antioxidant activity of propyl gallate in aqueous and lipid media: a theoretical study. *Phys. Chem. Chem. Phys.* **2013**, *15* (31), 13137−13146.
(35) Kalita, D.; Kar, R.; Handique, J. G. A theoretical study on the antioxidant property of gallic acid and its derivatives. *J. Theor. Comput. Chem.* **2012**, *11* (02), 391−402.
(36) Roginsky, V. Chain-breaking antioxidant activity of natural polyphenols as determined during the chain oxidation of methyl linoleate in Triton X-100 micelles. *Arch. Biochem. Biophys.* **2003**, *414* (2), 261−270.
(37) Denisova, T. G.; Denisov, E. T. Dissociation energies of OH bonds in natural antioxidants. *Russ. Chem. Bull.* **2008**, *57* (9), 1858−1866.
(38) de Souza, G. L.; Peterson, K. A. (2021). Benchmarking antioxidant-related properties for gallic acid through the use of DFT,

https://doi.org/10.1021/jasms.2c00017
J. Am. Soc. Mass Spectrom. XXXX, XXX, XXX−XXX

MP2, CCSD, and CCSD (T) approaches. *J. Phys. Chem. A* **2021**, *125* (1), 198−208.
(39) Ji, H.-F.; Zhang, H.-Y.; Shen, L. Proton dissociation is important to understanding structure-activity relationships of gallic acid antioxidants. *Bioorg. Med. Chem. Lett.* **2006**, *16*, 4095−4098.
(40) Rajan, V. K.; Muraleedharan, K. A computational investigation on the structure, global parameters and antioxidant capacity of a polyphenol, gallic acid. *Food Chem.* **2017**, *220*, 93−99.
(41) Škorňa, P.; Michalík, M.; Klein, E. Gallic acid: Thermodynamics of the homolytic and heterolytic phenolic O−H bonds splitting-off. *Acta Chim. Slov.* **2016**, *9*, 114−123.
(42) Đorovic, J.; Markovic, J. M. D.; Stepanic, V.; Begovic, N.; Amic, D.; Markovic, Z. Influence of different free radicals on scavenging potency of gallic acid. *J. Mol. Model.* **2014**, *20*, 2345.
(43) Kalita, D.; Kar, R.; Handique, J. G. A theoretical study on the antioxidant property of gallic acid and its derivatives. *J. Theor. Comput. Chem.* **2012**, *11*, 391−402.
(44) Masoud, M. S.; Hagagg, S. S.; Ali, A. E.; Nasr, N. M. Synthesis and spectroscopic characterization of gallic acid and some of its azo complexes. *J. Mol. Struct.* **2012**, *1014*, 17−25.
(45) Eslami, A. C.; Pasanphan, W.; Wagner, B. A.; Buettner, G. R. Free radicals produced by the oxidation of gallic acid: An electron paramagnetic resonance study. *Chem. Cent. J.* **2010**, *4* (1), 15.
(46) Mohammed-Ziegler, I.; Billes, F. Vibrational spectroscopic calculations on pyrogallol and gallic acid. *J. Mol. Struct.: THEOCHEM.* **2002**, *618* (3), 259−265.
(47) Billes, F.; Mohammed-Ziegler, I.; Bombicz, P. Vibrational spectroscopic study on the quantum chemical model and the X-ray structure of gallic acid, solvent effect on the structure and spectra. *Vib. Spectrosc.* **2007**, *43* (1), 193−202.
(48) Badhani, B.; Kakkar, R. DFT study of structural and electronic properties of gallic acid and its anions in gas phase and in aqueous solution. *Struct. Chem.* **2017**, *28* (6), 1789−1802.
(49) Blanksby, S. J.; Ellison, G. B. Bond dissociation energies of organic molecules. *Acc. Chem. Res.* **2003**, *36* (4), 255−263.
(50) Anstöter, C. S.; West, C. W.; Bull, J. N.; Verlet, J. R. The vitamin e radical probed by anion photoelectron imaging. *J. Phys. Chem. B* **2016**, *120* (29), 7108−7113.
(51) Marshall, M.; Zhu, Z.; Harris, R.; Collins, E.; Bowen, K. H. A Photoelectron spectroscopic study of the ascorbate and deprotonated ascorbate anions using an electrospray ionization source and a cryogenically cooled ion trap. *J. Phys. Chem. A* **2021**, *125*, 7699−7704.
(52) Gerhards, M.; Thomas, O. C.; Nilles, J. M.; Zheng, W.-J.; Bowen, K. H. Cobalt-benzene cluster anions: mass spectrometry and negative ion photoelectron spectroscopy. *J. Chem. Phys.* **2002**, *116*, 10247.
(53) Peláez, R. J.; Blondel, C.; Delsart, C.; Drag, C. Pulsed photodetachment microscopy and the electron affinity of iodine. *J. Phys. B-At. Mol. Opt.* **2009**, *42* (12), 125001.
(54) Luckoenig, E.; Morillon, C.; Vergès, J. Experimental and theoretical studies in atomic iodine-infrared arc spectrum observations, classification and hyperfine-structure. *Phys. Scr.* **1975**, *12* (4), 199−219.
(55) Frisch, M. J.; Trucks, G. W.; Schlegel, H. B.; Scuseria, G. E.; Robb, M. A.; Cheeseman, J. R.; Scalmani, G.; Barone, V.; Mennucci, B.; Petersson, G. A.; Nakatsuji, H.; Caricato, M.; Li, X.; Hratchian, H. P.; Izmaylov, A. F.; Bloino, J.; Zheng, G.; Sonnenberg, J. L.; Hada, M.; Ehara, M.; Toyota, K.; Fukuda, R.; Hasegawa, J.; Ishida, M.; Nakajima, T.; Honda, Y.; Kitao, O.; Nakai, H.; Vreven, T.; Montgomery, J. A., Jr.; Peralta, J. E.; Ogliaro, F.; Bearpark, M.; Heyd, J. J.; Brothers, E.; Kudin, K. N.; Staroverov, V. N.; Keith, T.; Kobayashi, R.; Normand, J.; Raghavachari, K.; Rendell, A.; Burant, J. C.; Iyengar, S. S.; Tomasi, J.; Cossi, M.; Rega, N.; Millam, J. M.; Klene, M.; Knox, J. E.; Cross, J. B.; Bakken, V.; Adamo, C.; Jaramillo, J.; Gomperts, R.; Stratmann, R. E.; Yazyev, O.; Austin, A. J.; Cammi, R.; Pomelli, C.; Ochterski, J. W.; Martin, R. L.; Morokuma, K.; Zakrzewski, V. G.; Voth, G. A.; Salvador, P.; Dannenberg, J. J.; Dapprich, S.; Daniels, A. D.; Farkas, O.; Foresman, J. B.; Ortiz, J. V.; Cioslowski, J.; Fox, D. J. *Gaussian 09, Revision D.01*; Gaussian, Inc.: Wallingford, CT, 2013.
(56) Zhao, Y.; Truhlar, D. G. The M06 suite of density functionals for main group thermochemistry, thermochemical kinetics, noncovalent interactions, excited states, and transition elements: two new functionals and systematic testing of four M06-class functionals and 12 other functionals. *Theor. Chem. Acc.* **2008**, *120* (1−3), 215−241.
(57) Grimme, S.; Antony, J.; Ehrlich, S.; Krieg, H. A consistent and accurate ab initio parametrization of density functional dispersion correction (DFT-D) for the 94 elements H-Pu. *J. Chem. Phys.* **2010**, *132* (15), 154104.
(58) Dunning, T. H., Jr. Gaussian basis sets for use in correlated molecular calculations. I. The atoms boron through neon and hydrogen. *J. Chem. Phys.* **1989**, *90* (2), 1007−1023.
(59) Kendall, R. A.; Dunning, T. H., Jr.; Harrison, R. J. Electron affinities of the first-row atoms revisited. Systematic basis sets and wave functions. *J. Chem. Phys.* **1992**, *96* (9), 6796−6806.
(60) Ervin, K. M.; Ho, J.; Lineberger, W. C. Ultraviolet photoelectron spectrum of nitrite anion. *J. Phys. Chem.* **1988**, *92* (19), 5405−5412.
(61) Ervin, K. M.; Ramond, T. M.; Davico, G. E.; Schwartz, R. L.; Casey, S. M.; Lineberger, W. C. Naphthyl Radical: Negative ion photoelectron spectroscopy, Franck- Condon simulation, and thermochemistry. *J. Phys. Chem. A* **2001**, *105* (48), 10822−10831.

https://doi.org/10.1021/jasms.2c00017
J. Am. Soc. Mass Spectrom. XXXX, XXX, XXX−XXX